COBEM 2023 27TH INTERNATIONAL CONGRESS OF MECHANICAL ENGENEERING

ABCM Brazilian Society of Mechanical Sciences and Engineering
27th ABCM International Congress of Mechanical Engineering
December 04-08, 2023, Florianópolis-SC, Brazil

COB-2023-251
NUMERICAL ANALYSIS OF THE MAGNETIC FLUX DENSITY PROFILE IMPACT ON THE TOTAL POWER PRODUCED BY A LINEAR THERMOMAGNETIC MOTOR

Clara Estillac Leal Silva [1]
Paulo Vinicius Trevizoli [2]
Universidade Federal de Minas Gerais, Departamento de Engenharia Mecânica - DEMEC. Av. Antônio Carlos, 6627 - Pampulha, Belo Horizonte, MG, Brasil
[1] claraestillacls@ufmg.br
[2] trevizoli@demec.ufmg.br

Abstract. *Thermomagnetic motors can be applied to convert low-grade thermal energy waste into mechanical energy, i.e., force or torque. The present work proposes a mathematical model to simulate a linear thermomagnetic motor designed and built at Universidade Estadual do Maringá (UEM). The mathematical model is numerically implemented using the finite volume method, and solves the energy equation to a porous media coupled to the thermomagnetic properties of Gd. After a preliminary comparison with the available experimental data, the model is used to investigate the influence of the magnetic flux density profile on the motor performance. Four different profiles, in addition to the reference one, are investigated. The output results are the cycle period, the maximum displacement, and the power produced by the motor. The results showed that the profile with a constant flux density gradient profile is the ideal case for the thermomagnetic motor, producing a power of 8.298 W, which is, approximately, 127.5% higher than the power produced by the reference profile. Furthermore, higher flux density gradients showed to be more important than larger total displacements and lower cycle periods.*

Keywords: *energy harvesting, thermomagnetic motors, heat transfer in porous media, numerical solution, magnetic flux density gradient*

1. INTRODUCTION

A possible solution to mitigate the increasing demand for energy is to enhance the efficiency of conventional energy systems, in which the conversion processes occur in the presence of different types of losses and irreversibilities. Low-grade thermal wastes, at temperatures below 100ºC, is one of the most abundant kind of heat losses in industries and in thermal power plants (Forman *et al.*, 2016). However, this energy is often rejected to the environment because of its low exergetic efficiency. Energy harvesters are devices specifically employed to recover low-grade heat waste and convert it to usable energy and can be associated in cogeneration with conventional systems to increase its efficiency (Kishore and Priya, 2018). In this context, thermomagnetic motors is one of the most promising types of energy harvesters and can convert the low-grade thermal waste into mechanical energy (Kitanovski, 2020).

Thermomagnetic motors (TMM) rely on the dependence of the magnetic properties on temperature and the applied magnetic field of a soft magnetic material (MM) around its Curie (transition) Temperature (T_{Curie}). Hence, if heat is supplied to the MM, it changes its magnetic phase to a non-magnetic phase (eg., paramagnetic); in turn, if heat is removed from the MM, it comes back to the ferromagnetic state.

To explain how a TMM operates, consider that a TMM is primarily composed of a permanent magnet magnetic circuit (MC), the MM arranged in a heat exchanger, a heat source, a heat sink, and a fluid flow system. Initially, the ferromagnetic material is positioned on the high-applied magnetic field region. Then, heat is transferred to the MM along a warm blow period, supplied by the heat source. As the magnetic force is reduced due to the shifting to a non-magnetic phase, the MM material can be removed from the high field region. Now, subjected to a low field (but, non-zero field), the MM is cooled down by a cold blow, from the heat sink. As the ferromagnetic phase is restablished, the MM is moved back to the initial (high-field) position, and the cycle can start over again. Thereby, the MM experiences a periodic magnetic phase change (ferro to paramagnetic) which guarantees a non-balance between the forces acting on the heat exchangers, which results in a linear or rotary motion. The magnetic force produced is proportional to the MM mass, its specific magnetization, and the MC magnetic density flux gradient.

Recent works on TMM involved experimental setups and simulations. In the matter of experimental works, Murakami and Nemoto (1972) developed a rotary TMM prototype. However, the authors concluded that for obtaining reasonable efficiencies values MC with higher magnetic fields and MM with higher specific magnetization values would be needed. Thereafter, Takahashi *et al.* (2006) designed a rotary TMM with three high magnetic field regions. A FeNiCr alloy was

used as the MM, while water and air were evaluated as the working fluid. The device presented a 3,7 W produced power and a rotational speed of 0,4 RPS. Mehmood *et al.* (2021) developed a TMM with two field regions and used Gd as the MM. The author reported a 1 W produced power at 220 RPM speed. Kaneko *et al.* (2021) designed and built a purely magnetic linear TMM. The device consists of a double-C shape permanent magnet MC, that generates two high field regions, and two magnetic heat exchangers filled with spherical particles of Gd in a packed-bed arrangement. The warm and cold blows flows through the porous media along different periods of the cycle. This way, the Gd experiences a periodic change of its magnetic phase, establishing a non-balance between the magnetic forces acting on each heat exchanger, which results in a linear motion.

In regards to numerical works, Alves *et al.* (2013) simulated a Curie's Wheel (rotary) using solar energy as the heat source and compared the performance for three different MM: Gadolinium (Gd), FeNi and MnAs alloys. The heat transfer model was implemented via the finite differences method. The MnAs alloy, first-order magnetocaloric material (Gutfleisch *et al.*, 2016), presented lower magnetic forces combined with shorter cycle periods. Hey *et al.* (2022b) developed a mathematical model associated with an optimization procedure having the maximum total produced power as the objective function. The analysis resulted in an optimum TMM with a produced power of 88 W. Gabrielyan *et al.* (2013) implemented in ANSYS a 3D model of a disk-shaped TMM using Gd as the MM. Water was used to generate a temperature gradient that associated with the magnetic field gradient generates rotary motion. Kishore *et al.* (2020) simulated a linear TMM varying the temperatures of the heat source and sink and evaluated its impacts on the motor performance. Evaristo *et al.* (2022) proposed a linear TMM counterbalanced by the gravitational force. The authors evaluated the impact of the internal demagnetization fields on the motor performance. The simulations presented a produced power of 0,3 W and a cycle period of 20 s, resulting from the poor heat transfer properties of circular channel geometry considered in the magnetic heat exchanger. Corrêa *et al.* (2023) used the finite volume method to simulate a spring-returned TMM, coupled to an optimization routine. Parameters such as the heat exchanger length, the spring constant value, the heat source temperature, and the fluid mass flow rate have been optimized striving to reduce the total entropy generation and the back work ratio (BWR). The optimized TMM presented a 5 W liquid power and a 12% BWR. Lastly, Hey *et al.* (2022a)) simulated and compared a linear and a rotating TMM. The linear motors have shown to be more efficient, yet the rotative ones are capable of operating with a smaller temperature difference between the heat source and the heat sink.

The present work proposes a 1D mathematical model, implemented using the Finite Volume Method (Maliska, 2004), to simulate the heat transfer and the linear motion of a TMM similar to the concept proposed by Kaneko *et al.* (2021). The transient model couples the Gd magnetic properties with the porous media heat transfer energy equations, considering the demagnetization losses and the magnetocaloric effect (MCE) (Smith *et al.*, 2012). The fluid and solid properties depend on the temperature and the resulting magnetic field. Four different magnetic flux density distributions are proposed, taking as reference the experimental magnetic field measured in Kaneko *et al.* (2021) apparatus. The maximum and minimal values of each profile are the same as the reference one, allowing a more reliable analysis. Then, simulations are performed to evaluate the impact of the magnetic flux density gradient profile at the TMM performance parameters, such as the cycle period, the heat exchangers displacements, and the produced power.

2. METHODOLOGY

2.1 Experimental setup

The magnetic circuit from the TMM designed by Kaneko *et al.* (2021) (Fig. 1a) is double-C shaped and has a magnetic field generated by NdFeB permanent magnets. Soft magnetic materials, with high magnetic permeability, are used to guide the magnetic field toward the magnetic gap, increasing the magnetic field intensity. Specific information about the MC characterization can be found at Kaneko *et al.* (2019). In regards to the magnetic heat exchangers (MHEx), the two units are made of G10 fiberglass shell, with 16 mm diameter and 81 mm length, filled with Gd spheres establishing a porosity of 37%, i.e., a total MM mass of 114,5 g each.

The MHEx displacement occurs along the magnetic flux density gradient profile, x-axis of Fig. 2. The heat exchanger at a temperature lower than the T_{Curie} is attracted to the high magnetic field region (red circle at Fig. 1b), hence the other heat exchanger, at a temperature higher than T_{Curie}, is displaced to the low magnetic field region (blue circle at Figure Fig. 1b).

2.2 Mathematical model

The experimental apparatus involves a heat source and a heat sink, two pumping systems, solenoid valves and instrumentation to control the flow rate and temperature. Due to the complexity of the overall setup, some simplifying hypotheses have to be made to limit the analysis domain: (i) the fluid at the heat source and sink temperatures are considered to be uniform; (ii) neither the pumps efficiencies nor the power consumption by the solenoid valves are considered; (iii) pressure drop at the piping and valves are not considered; (iv) heat gain/losses throughout the piping and valves are

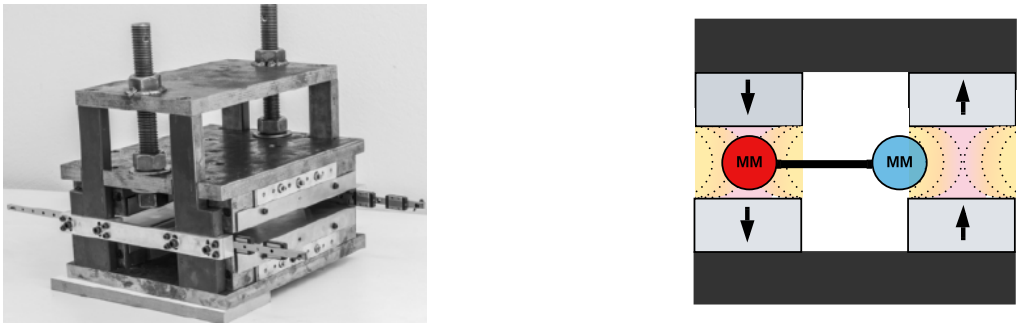

(a) (b)

Figure 1: Magnetic Circuit in study. Adapted from Kaneko *et al.* (2019)

not considered. Combining (i) to (iv) limits the MHex domain to 1D along the longitudinal axis, while the magnetic field gradient is along the x-axis (transversal to the longitudinal).

The mathematical model couples the non-equilibrium heat transfer equations in a porous media and the Gd thermo-magnetic phenomena. For the model, the following hypotheses are considered: (v) the warm and cold blow temperatures are prescribed and equal to the heat source and sink ones, respectively; (vi) the flow is parallel to the MHEx longitudinal axis; (vii) the flow rate is prescribed; (viii) the flow rate is instantaneous, which means that the flow velocity is constant during its periods; (viv) the magnetic field is constant throughout the entire MHEx length; (x) the MHEx displacement occurs uniquely along the x-axis, in accordance to the magnetic flux density profile. Thereby, the mathematical model domain is fully defined.

2.2.1 Heat transfer equations

In addition to those, other simplifying hypotheses are also applied to the energy conservation equations: (a) the flow is unidimensional and isochoric; (b) the Gd thermal conductivity and density are constants; (c) the Gd spheres have uniform diameter; (d) the porosity is constant throughout the MHex bed. In this way, the simplified fluid (Eq. 1) and solid (Eq. 2) energy equations are as follows (Kaviany, 1995):

$$\varepsilon \frac{\partial T_f}{\partial t} = -\frac{h\beta}{\rho_f C_{p_f}} \left(T_f - T_s\right) - u_D \frac{\partial T_f}{\partial z} + \varepsilon \left(\frac{k_f}{\rho_f C_{p_f}} + D_{II}\right) \frac{\partial^2 T_f}{\partial z^2} + \frac{1}{\rho_f C_{p_f}} \left|\frac{\partial P}{\partial z} u_D\right| \tag{1}$$

$$(1-\varepsilon) \frac{\partial T_s}{\partial t} = -\frac{h\beta}{\rho_s C_{p_s}} \left(T_s - T_f\right) + (1-\varepsilon) \frac{k_s}{\rho_s C_{p_s}} \frac{\partial^2 T_s}{\partial z^2} \tag{2}$$

The subscripts *f* and *s* refer to fluid and solid, respectively, and: ε is the spheres packed bed porosity, β is the superficial area density, *t* is the time, ρ is the specif mass, C_p is the specif heat, *z* is the axial position, *k* is the thermal conductivity and μ is the viscosity. Following, u_D is the Darcy's velocity, considered as an average value due to the resemblance between a porous media flow at a macroscopic scale and an inviscid flow. This way, u_D can be calculated by Eq.3, where $\dot{m}$ is the mass flow rate and A_c the cross-section area.

$$u_D = \frac{\dot{m}}{\rho_f A_c} \tag{3}$$

Also, D_{II} is the longitudinal dispersion, which aims to correct the fluid axial conduction as the hydrodynamic mixture at the porous level due to a forced flow can present a relevant thermal dispersion. Therefore, it must be considered at the heat conduction term and it is calculated using the Koch and Brady (1985) correlation. The convection heat transfer coefficient (*h*) is obtained using Pallares and Grau (2010) correlation. Lastly, $\frac{\partial P}{\partial z}$ is the longitudinal pressure gradient calculated by Ergun (1952) correlation, corrected by Macdonald *et al.* (1979), valid for Reynolds numbers based on the particle diameter lower than 1000.

The fluid employed to exchange heat with the Gd particles is a mixture of water and ethylene glycol at an 80/20%v. Its properties are a function of the temperature. As mentioned previously, Gd density and thermal conductivity are considered constant, but its specific heat is a function of the temperature and the resultant magnetic field.

The model boundary condition for the fluid phase at $z = 0$ is a mass entrance condition, with a prescribed temperature and mass flow rate. For the warm blow, the temperature is equal to the heat source, and for the cold blow is equal to the heat sink one. At $z = L$ is a mass outlet boundary condition (parabolic condition), hence ($\frac{\partial T}{\partial z} = 0$). For the solid phase, both conditions at $z = 0$ and $z = L$ are adiabatic, i.e., (-k $\frac{\partial T}{\partial z} = 0$).

2.2.2 Magnetocaloric effect

Along the thermodynamic cycle of the TMM motor, every moment that the MHex changes its position along the x-axis, the MM experiences an external field change. However, gadolinium presents a significant magnetocaloric effect (MCE) (Dan'Kov *et al.*, 1998) at the TMM operating temperature range, hence, its contribution must be considered in the heat transfer model.

The MCE is implemented as a function of time (t) and the MHEx position (z), because the MM temperature and the resulting magnetic field are also functions of those parameters. Considering that the external field variation is adiabatic, a discrete implementation is used (Nielsen *et al.*, 2011). In this implementation, as shown in Eq. 4, the MM temperature is corrected by a ΔT_{ad} whenever it is subjected to a magnetic field change.

$$T_s(t+\Delta t, z) = T_s(t,z) + \Delta T_{\text{ad}}(\Delta\mu_0 H_{int,res}(t,z), T_s(t,z)) \tag{4}$$

2.3 Numerical implementation

2.3.1 Heat transfer model implementation

The energy equations, Eq. 1 and Eq. 2, are solved using Finite Volume Method ((Maliska, 2004)). The transient contributions are implemented by the fully implicit scheme. The diffusive and advective terms at the fluid energy equation (Eq. 1) are approximated by the Weighted Upstream Differencing Scheme (WUDS) and the solid energy equation (Eq. 2) is solved by the Central Difference Scheme (CDS). The boundary conditions are implemented via the fictitious domains method. As it comes to a 1D domain, there are only two additional volumes in each phase.

The TriDiagonal Matrix Algorithm (TDMA), also known as Thomas Algorithm, is used to solve energy equations. As a line-by-line method, it presents direct solutions for 1D domains. However, the equations are coupled by the interstitial heat transfer contribution and, this way, an iterative solution is necessary, where the convergence criteria is set at 10^{-4}. The solver stops when the periodic steady state is achieved when comparing two consecutive cycles, respecting the convergence criteria of 10^{-8}.

A mesh independence analysis is conducted to ensure the stability and convergence of the obtained results. A total of five spatial meshes: 10, 10^2, 5.10^2, 10^3 and 2.10^3, are evaluated; and five different time steps are evaluated: 10^{-2} s, 5.10^{-3} s, 10^{-4} s, 5.10^{-5} s and 10^{-5} s. The combination of 500 volumes and a time step of 10^{-3} s presented produced power values with errors less than 1% in comparison with a more refined mesh (1000 volumes and 10^{-4} s) associated with lower computational costs.

2.3.2 Magnetic heat exchangers motion

The magnetic force acting on the MHEx can be calculated by the Eq. 5, where *V* is the MHex total volume and $\frac{\partial B}{\partial x}$ is the applied magnetic flux density gradient along the *x* axis.

$$F_{mag} = -\left(1-\varepsilon\right)\rho_s V M\left(T, B_{int}\right)\frac{dB}{dx} \tag{5}$$

Since the MM temperature and the magnetic flux density varies at each finite volume, the magnetic force also needs to be calculated for each one. The total force acting on the MHEx is the sum of the individual forces acting on every single finite volume.

The system position is defined by the balance between the forces acting on the two MHExs. As the magnetic force is a function of the MHEx position along the x-axis, thus, the process becomes iterative for each time step. Initially, the forces are calculated and compared, then the system is displaced by Δx at the higher force direction. The process is repeated until the balance is verified. In this work, an absolute residual force balance of 10^{-6} N is taken as a convergence condition.

2.4 Perfomance metrics

The main output results obtained from the simulations are cycle period, MHEx total displacement, and TMM produced power. All of them are calculated after the simulation has reached the periodic steady state. The produced power is determined by Eq. 6, where $\bar{F}_{res}X$ is the mean magnetic force acting on one of the MHEx, *X* is the system total displacement during one cycle and t_{cycle} the cycle period.

$$\dot{W}_p = \frac{\bar{F}_{res}X}{t_{cycle}} \tag{6}$$

2.5 Magnetic flux density profiles

Four different magnetic flux density profiles along with their gradients (Fig. 2a and Fig. 2b, respectively) are elaborated and implemented to evaluate their impact on the TMM performance. The maximum and minimal flux density values of each on are kept at the same intensities as the original one proposed by Kaneko *et al.* (2021): 0.85 T (maximum) and 0.04 T (minimum). This allowed a more reliable analysis, as the flux density gradient profile is the main impact on the output results.

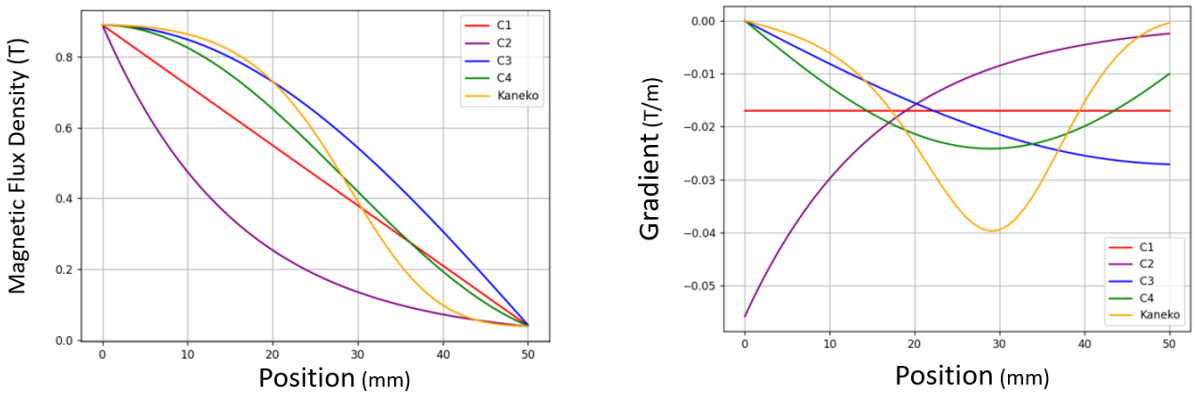

(a) (b)

Figure 2: Proposed curves: (a) magnetic flux density profiles; (b) magnetic flux density gradient profiles

Combinations of the new curves were also considered to establish non-symmetric flux density and gradient profiles. As so, one MHEx is attracted to the high field region under the influence of one magnetic flux density profile while the other is removed from the high field region under the influence of a second magnetic flux density profile. Kaneko *et al.* (2021) profile are also included in this evaluation.

3. RESULTS AND DISCUSSION

3.1 Comparison with experimental results

Simulation results for the cycle period, MHEx total displacement, and produced power are compared with Kaneko *et al.* (2021) data (Tab. 1). The temperatures of the heat sink and heat source are 0 ºC and 50 ºC, respectively, while the cold blow rate is 39.4 L/h and the warm blow rate is 82.4 L/h.

Table 1: Comparison between experimental and simulation results.

Parameter	Simulation	Experimental
Cycle period (s)	2,822	2,000
Total displacement (mm)	37,8	40,0
Produced power (W)	1,018	0,410

The cycle period reported by Kaneko *et al.* (2021) is lower than the one obtained as a simulation result. That difference can be justified by the fact that the experimental cycle period is an input parameter (by adjusting the time to open/close the solenoid valves), while in the simulation it is an output result. Also, the total displacement reported by Kaneko *et al.* (2021) is a theoretical value that has not been experimentally measured, this way the comparison with the numerical result is not reliable.

Even with a higher total displacement and a shorter cycle period, the experimental result presented a lower produced power. This difference can be attributed to: (i) the total displacement's uncertainties; (ii) the employment of a mechanism to convert the linear motion into rotational in the experimental setup, which may have introduced a severe mechanical loss to the system; (iii) the use, in the simulation, of the Gd ideal properties; (iv) the equations to evaluate the magnetic work in the mathematical model. However, these are the only experimental data available, and thus, a more in-depth experimental evaluation is necessary to perform the mathematical model validation.

Despite the differences, the compared results have the same order of magnitude, and their divergences can be justified. Hence, even though it is not fully validated, the proposed mathematical model is consistent and can be used to perform important evaluations, such as the impact of the magnetic flux density profile on the TMM performance, as follows.

3.2 Influence of the magnetic flux density profile

Table 2 presents the output results for all proposed combinations of the magnetic flux density profiles (see Fig. 2a). The simulations considered a fixed mass flow rate of 60 kg/h for both warm and cold blows, as well the temperatures of the hot and cold reservoirs at 50ºC and 0ºC. It is important to emphasize that all the profiles presented, besides the reference one by Kaneko *et al.* (2021), are theoretical.

Table 2: Output results for the different magnetic field profiles.

Magnetic Field	Cycle Period [s]	Produced Power [W]	Displacement [mm]
C1 - C1	0,872	8,298	40
C3 - C3	1,846	2,229	36,4
C4 - C4	1,582	3,243	38,8
Kaneko - Kaneko	1,934	3,647	37,8
C1 - Kaneko	1,468	2,739	38,1
C3 - Kaneko	1,829	2,576	35,9
C4 - Kaneko	1,678	3,357	37,6
C1 - C3	1,262	4,361	39,4
C1 - C4	1,316	4,091	39,4
C3 - C4	1,681	2,886	38,1

Notice that curve C2 does not have its results at Tab. 2 because the motor is not able to operate under that flux density profile. As it can be observed in Fig. 2b, the magnetic flux density gradient has a very high-intensity value around $x = 0$, and a very low-intensity at $x = 50$ mm. This way, even though the MHEx at $x = 0$ is paramagnetic, and the MHEx at $x = 50$ mm is ferromagnetic, the magnetic force on the latter is not high enough to move the paramagnetic MHEx out of the high-field region. As a result, no motion is observed, and this sort of flux density profile must be avoided when designing permanent-magnets magnetic circuits for TMM applications.

The linear magnetic flux density gradient C1, on the other hand, presents the highest produced power. This can be explained by the MHEx displacement during the cycle, as in Fig. 3a, which is compared with the reference profile by Kaneko *et al.* (2021) in Fig. 3b. The MHex remains still during the whole heat exchange process until it reaches a temperature that unbalance the magnetic forces. Then the system moves instantaneously to the maximum displacement position, where it remains throughout the following blow period. When comparing with Fig. 3b, the position of the MHEx varies along the blow periods, respecting the balance of magnetic forces, thus, there are several intermediate equilibrium positions between $x \approx 0$ and $x \approx 40$ mm. In this way, it can be concluded that C1 is the ideal case for a TMM, and this sort of flux density profile should be the target one when designing permanent-magnets magnetic circuits for such application.

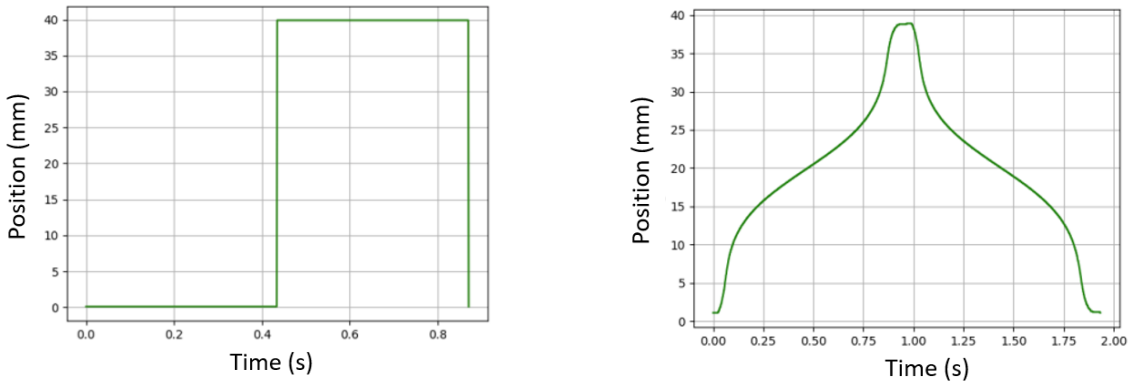

(a) (b)

Figure 3: MHEx displacement along the cycle: (a) C1 magnetic flux density profile; (b) Kaneko *et al.* (2021) magnetic flux density profile.

Fig. 4a and 4b present the temperature transient at different positions (represented by the different finite volumes) along the MHEx length, considering the C1 magnetic flux density profile. Due to its short cycle period, the last finite volumes (V375 to V500) are always out of phase in relation to the temperature of the respective blow and, thus, it will

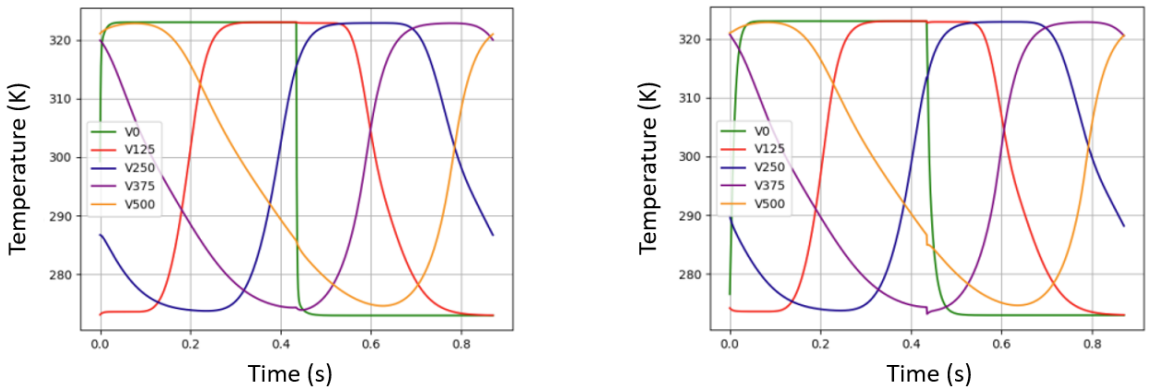

(a) (b)

Figure 4: Temperature transients at different positions along the MHEx length, considering the C1 magnetic flux density profile: (a) fluid phase; (b) solid phase.

not achieve thermal equilibrium with the heat source and sink. This is a clear opportunity to optimize the MHEx length, reducing the mass of magnetic material and permanent magnets, as well as potentially shortening the cycle period.

All the asymmetric magnetic flux density gradient profiles resulting from the combination with the C1 curve presented lower cycle periods than the symmetric ones. For the C3 and C4 curves, that combination also resulted in a higher produced power, which is not observed in the combination of Kaneko *et al.* (2021) profile with C1.

In addition, C3 and C4 profiles presented results close to the reference profile. However, even though its cycle period is higher than the others, the reference profile still presents a higher produced power. This is justified by its higher gradient intensity in the region $20 \leq x \leq 38$ mm (see Fig. 2b).

4. CONCLUSIONS

The present work proposed a numerical analysis of a purely magnetic thermomagnetic motor previously designed and built for Kaneko *et al.* (2021). The mathematical model couples the heat transfer in a porous media and the Gd thermomagnetic phenomena. The Finite Volume Method was employed for the model implementation, using the TDMA line-by-line as solver.

Initially, the operational conditions presented by Kaneko *et al.* (2021) were considered as input parameters in the simulation, in a try to validate the proposed model. Although some differences were observed and explained with respect to the available experimental data, the numerical results are relatively close, and the model could be further validated with new and more detailed experimental data.

Next, four different magnetic flux density profiles were elaborated and implemented. The output results for the cycle period, MHEx's total displacement, and produced power are compared between the different profiles, as well with the reference one by Kaneko *et al.* (2021), and their non-symmetric combinations. The linear magnetic density profile with a constant gradient has shown to be the ideal condition for the TMM operation, with a produced power of 8,3 W. In this way, when designing a novel magnetic circuit to be employed in a TMM, the magnetic flux density profile must be as close to a linear trend.

Finally, although the proposed mathematical model still needs improved and fully validated, it has shown to be versatile as it is simple to implement and simulate new magnetic field distributions. Thereby, it can be considered a powerful tool in the decision making process when designing new TMM concepts.

ACKNOWLEDGEMENTS

The authors are grateful for the financial support from Fundação de Amparo à Pesquisa do Estado de Minas Gerais (FAPEMIG) through Grant No. APQ-00877-21 (Demanda Universal); Conselho Nacional de Desenvolvimento Científico e Tecnológico (CNPq) through Grant No. 405970/2021-8; The National Institute of Science and Technology (Refrigeration and Thermophysics) through grant from Conselho Nacional de Desenvolvimento Científico e Tecnológico (CNPq 404023/2019-3).

REFERENCES

Alves, C., Colman, F., Foleiss, G., Vieira, G. and Szpak, W., 2013. "Numerical simulation and design of a thermomagnetic motor". *Applied thermal engineering*, Vol. 61, No. 2, pp. 616–622.

Corrêa, L.S., Rowe, A. and Trevizoli, P.V., 2023. "Thermodynamic optimization of a linear thermomagnetic motor". *Applied Thermal Engineering*, Vol. 219, p. 119344.

Dan'Kov, S.Y., Tishin, A., Pecharsky, V., Gschneidner, K. *et al.*, 1998. "Magnetic phase transitions and the magnetothermal properties of gadolinium". *Physical Review B*, Vol. 57, No. 6, p. 3478.

Ergun, S., 1952. *Fluid Flow Through Packed Columns*. Contribution (Carnegie Institute of Technology, Coal Research Laboratory).

Evaristo, E., Colman, F., Alves, C. and Trevizoli, P., 2022. "Mathematical modelling and simulation results of a linear thermomagnetic motor with gravity return". *Journal of Magnetism and Magnetic Materials*, Vol. 544, p. 168668.

Forman, C., Muritala, I.K., Pardemann, R. and Meyer, B., 2016. "Estimating the global waste heat potential". *Renewable and Sustainable Energy Reviews*, Vol. 57, pp. 1568–1579. ISSN 1364-0321. doi: https://doi.org/10.1016/j.rser.2015.12.192.

Gabrielyan, D., Semenov, V. and Martirosov, D., 2013. "Analysis of nonstationary heating and cooling of a thermomagnetic engine gadolinium working element". *Russian Aeronautics (Iz VUZ)*, Vol. 56, pp. 266–273.

Gutfleisch, O., Gottschall, T., Fries, M., Benke, D., Radulov, I., Skokov, K.P., Wende, H., Gruner, M., Acet, M., Entel, P. *et al.*, 2016. "Mastering hysteresis in magnetocaloric materials". *Philosophical Transactions of the Royal Society A: Mathematical, Physical and Engineering Sciences*, Vol. 374, No. 2074, p. 20150308.

Hey, J., Tan, J. and Tan, Z., 2022a. "An evaluation of thermomagnetic motors for heat energy harvesting". In *2022 IEEE/ASME International Conference on Advanced Intelligent Mechatronics (AIM)*. IEEE, pp. 1347–1354.

Hey, J., Repaka, M., Li, T. and Tan, J.L., 2022b. "Design optimization of a rotary thermomagnetic motor for more efficient heat energy harvesting". *Energies*, Vol. 15, No. 17, p. 6334.

Kaneko, G., Conceição, W., Colman, F., Cocci, A., Alves, C., Pupim, G., Kubota, G., Oliveira, V. and Trevizoli, P., 2021. "Design and experimental evaluation of a linear thermomagnetic motor using gadolinium: Preliminary results". *Applied Thermal Engineering*, Vol. 186, p. 116472.

Kaneko, G., Souza, A., Moro, F., Colman, F., Conceição, W., Alves, C. and Trevizoli, P., 2019. "Design and assembling of a magnetic circuit for a thermomagnetic motor apparatus". *Journal of the Brazilian Society of Mechanical Sciences and Engineering*, Vol. 41, No. 10, pp. 1–11.

Kaviany, M., 1995. *Principles of Heat Transfer in Porous Media*.

Kishore, R. and Priya, S., 2018. "A review on low-grade thermal energy harvesting: Materials, methods and devices". *Materials*, Vol. 11, No. 8. ISSN 1996-1944. doi:10.3390/ma11081433.

Kishore, R.A., Singh, D., Sriramdas, R., Garcia, A.J., Sanghadasa, M. and Priya, S., 2020. "Linear thermomagnetic energy harvester for low-grade thermal energy harvesting". *Journal of Applied Physics*, Vol. 127, No. 4, p. 044501.

Kitanovski, A., 2020. "Energy applications of magnetocaloric materials". *Advanced Energy Materials*, Vol. 10. doi: https://doi.org/10.1002/aenm.201903741.

Koch, D.L. and Brady, J.F., 1985. "Dispersion in fixed beds". *Journal of Fluid Mechanics*, Vol. 154, p. 399–427.

Macdonald, I., El-Sayed, M., Mow, K. and Dullien, F., 1979. "Flow through porous media-the ergun equation revisited". *Industrial & Engineering Chemistry Fundamentals*, Vol. 18.

Maliska, C., 2004. *Transferência de calor e mecânica dos fluidos computacional*. Livros Tecnicos e Cientificos.

Mehmood, M.U., Kim, Y., Ahmed, R., Lee, J. and Chun, W., 2021. "Design and operation of a thermomagnetic engine for the exploitation of low-grade thermal energy". *International Journal of Energy Research*, Vol. 45, No. 10, pp. 15298–15311.

Murakami, K. and Nemoto, M., 1972. "Some experiments and considerations on the behavior of thermomagnetic motors". *IEEE Transactions on Magnetics*, Vol. 8, No. 3, pp. 387–389.

Nielsen, K., Tusek, J., Engelbrecht, K., Schopfer, S., Kitanovski, A., Bahl, C., Smith, A., Pryds, N. and Poredos, A., 2011. "Review on numerical modeling of active magnetic regenerators for room temperature applications". *International Journal of Refrigeration*, Vol. 34, No. 3, pp. 603–616. ISSN 0140-7007. doi:https://doi.org/10.1016/j.ijrefrig.2010.12.026. URL `https://www.sciencedirect.com/science/article/pii/S0140700711000053`.

Pallares, J. and Grau, F., 2010. "A modification of a nusselt number correlation for forced convection in porous media". *International Communications in Heat and Mass Transfer*, Vol. 37.

Smith, A., Bahl, C.R., Bjørk, R., Engelbrecht, K., Nielsen, K.K. and Pryds, N., 2012. "Materials challenges for high performance magnetocaloric refrigeration devices". *Advanced Energy Materials*, Vol. 2, No. 11, pp. 1288–1318.

Takahashi, Y., Yamamoto, K. and Nishikawa, M., 2006. "Fundamental performance of triple magnetic circuit type cylindrical thermomagnetic engine". *Electrical Engineering in Japan*, Vol. 154, No. 4, pp. 68–74.

5. RESPONSIBILITY NOTICE

The authors are solely responsible for the printed material included in this paper.